Journal of Alloys and Compounds 507 (2010) 317–321

Contents lists available at ScienceDirect

Journal of Alloys and Compounds

journal homepage: www.elsevier.com/locate/jallcom

Chemical synthesis of Cu(In) metal inks to prepare $CuInS_2$ thin films and solar cells

Guanbi Chen, Lei Wang, Xia Sheng, Hongjuan Liu, Xiaodong Pi, Deren Yang*

State Key Laboratory of Silicon Materials and Department of Materials Science and Engineering, Zhejiang University, Hangzhou 310027, People's Republic of China

ARTICLE INFO

Article history:
Received 7 May 2010
Received in revised form 23 July 2010
Accepted 27 July 2010
Available online 5 August 2010

Keywords:
Nanoparticles
Metal inks
$CuInS_2$ thin film
Solar cells

ABSTRACT

We report a chemical method to prepare Cu/In inks or Cu–In inks, from which $CuInS_2$ films are formed. Cu, In and Cu–In nanoparticles are initially synthesized by a polyol method, and then dispersed in solvents to form inks. Metal films are subsequently obtained by drop-casting the Cu inks and In inks in sequence or Cu–In inks directly. The sulfurization of the metal films is carried out in a tube with high sulfur vapors. The obtained $CuInS_2$ films are compact with large grains and pure phases. The band gap of the $CuInS_2$ film is determined to be ~1.45 eV, which is near the optimal band gap of the solar cell materials. Tentative $CuInS_2$ solar cell with an efficiency of 0.7% is fabricated.

1. Introduction

$CuInS_2$ (CIS) thin films with optical band gap of 1.5 eV are favored for the production of high-efficiency single-cell systems with large open circuit voltage and of top cells in tandem systems [1]. However, expensive vacuum equipments are employed in industrial production of CIS films, usually by subsequent evaporation of elemental layers (i.e. Cu, In, etc.), or simultaneous co-evaporation of these elements [2,3]. To reduce the cost of the thin-film solar cells non-vacuum techniques are intensively studied [4–6]. Among a variety of non-vacuum techniques, nanoparticle-based ink printing is attractive, given the convenience for large-scale production and sufficient utilization of materials [7–9]. Thereinto, nanoparticles play an important role in the preparation of inks.

Up to now, three methods have mainly been reported for the preparation of nanoparticles related to CIS films. The first is that CIS particles are directly synthesized by sol–gel or mechanical alloying (MA). However, the sol–gel process leads to porous CIS aggregates, which are readily oxidized [10]. Moreover, large distribution of particle sizes is also a serious problem in the MA [11]. The second is that metal precursors such as metal oxides or metal salts are initially prepared. After reduction and selenization/sulfurization, separate particles are sintered together to form integrated films. However, since metal-oxide impurities may remain in the films to initiate cracks and shrinkages, an extra reduction process must be carried out [12]. The third is that fine Cu–In alloy particles are produced by a physical top-down method (MA or gas atomization) [13]. In this case, again, the MA cannot lead to a narrow size distribution of Cu–In particles. It is usually difficult to handle gas atomization, especially given the fact that the boiling point of In is low [14]. Therefore, simple and cost-effective methods to prepare particles related to CIS films still need to be developed.

In this paper, we present a novel low-cost method to prepare Cu, In or Cu–In nanoparticles, which then are used to fabricate CIS films. Modified polyol method is successfully employed to synthesis metal nanoparticles. The metal nanoparticles are then dispersed in solvents to form inks. Later on, metal films can be subsequently obtained by drop-casting Cu inks and In inks in sequence or Cu–In inks, analogous to the subsequent or simultaneous evaporation in industry, respectively. Finally, the sulfurization of the metal films leads to the formation of CIS films, which are compact with large grains and pure phases. CIS solar cell is also prepared and investigated.

2. Experimental

Analytical grade reagents were used in this work. They were indium trichloride, $InCl_3{\cdot}4H_2O$; copper dichloride, $CuCl_2{\cdot}2H_2O$; poly(vinyl pyrrolidone) (PVP, K30); sodium borohydride ($NaBH_4$); diethylene glycol (DEG); tetraethylene glycol (TEG); ethylene glycol (EG), 2-methoxyethanol (MeEtOH), and methyl alcohol (MeOH); sulfur (S). The nanoparticles were synthesized by an approach similar with the commonly used polyol method [15]. 1 mmol metal salt ($InCl_3{\cdot}4H_2O$ or $CuCl_2{\cdot}2H_2O$) and 0.2 g PVP were firstly dissolved into 25 ml DEG under N_2 at 140 °C. Some amount of freshly made $NaBH_4$/TEG solution (0.2 g in 8 ml TEG) was added. The particles continued to grow for some time (3 min for In particles and 30 min for Cu particles). As for the synthesis of Cu–In nanoparticles, the same experimental procedure was used, in which equal amount of Cu and In salts were added. The products were separated by centrifugation and washed several times by ethanol.

* Corresponding author. Tel.: +86 571 87952752; fax: +86 571 87952322.
E-mail address: mseyang@zju.edu.cn (D. Yang).

0925-8388/$ – see front matter © 2010 Elsevier B.V. All rights reserved.
doi:10.1016/j.jallcom.2010.07.190

The synthesized nanoparticles were mixed with a stock solvent (EG/MeEtOH/MeOH = 5:4:1 by weight). In the mixtures the nanoparticles were 20% by weight. Inks were formed by ultrasonicating or grinding the mixtures. Glass substrates were ultrasonically cleaned in a water–detergent solution and then washed with acetone and ethanol. They were finally dried in a furnace at 80 °C. We used two methods to prepare metal films on glass substrates denoted as stacking and mixing methods. In the stacking method the films were prepared by drop-casting Cu inks and In inks in sequence (stacking method 1) or In inks and Cu inks in sequence (stacking method 2). In the mixing method the films were formed by drop-casting Cu–In inks. After each drop-casting, a drying process at 80 °C for 30 min was performed. The metal films were loaded into a quartz–tube furnace in sulfur atmosphere under the protection of nitrogen gas. The furnace temperature was ramped from room temperature to 250 °C in 0.5 h and stayed for 20 min to eliminate organic residuals. The temperature was then ramped to 550 °C in 1 h and held for another 1 h to complete the sulfurization. The CIS solar cell was prepared with a structure of Ag/ITO/i-ZnO/CdS/CIS/Mo following the custom procedures.

X-ray diffraction (XRD) was carried out to study the crystalline structures of all the samples by using an X'Pert PRO (PANalytical) diffractometer equipped with a Cu Kα radiation source. Data was collected by step-scanning of 2θ from 20° to 70° with a step of 0.02° and counting time of 1 s per step. Morphology of the samples was investigated by scanning electron microscopy (SEM, Hitachi S4800). The optical transmittances (T) of the finished films were measured by using a UV–vis spectrophotometer (Hitachi Model U-4 100). ABET solar simulator was used as the light source and certificated with a monocrystal Si solar cell. I–V characteristic of the device was carried on an ammeter of Keithley 2400.

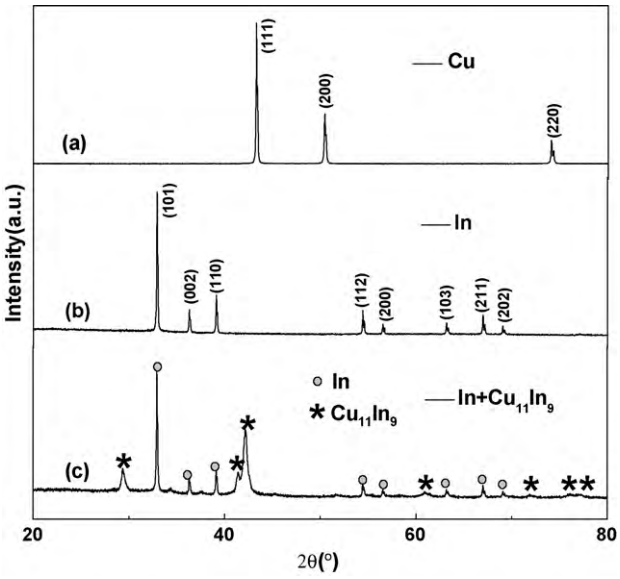

Fig. 1. XRD diffraction patterns of (a) Cu nanoparticles, (b) In nanoparticles and (c) Cu–In nanoparticles.

3. Results and discussion

In the experiments, Cu, In or Cu–In nanoparticles are firstly synthesized, respectively. The XRD pattern of the Cu nanoparticles shown in Fig. 1(a) indicates that the Cu is face-centered-cubic (fcc) crystal structure, the same as that in Ref. [16]. Their SEM image shown in Fig. 2(a) displays that the Cu nanoparticles are uniform with particle size of about 50 nm. Moreover, In nanoparticles with tetragonal phase are synthesized, as indicated from the XRD pattern in Fig. 1(b). In the pattern, no preferred orientation is found, indicating that the In products follows an isotropic growth process. The SEM image shown in Fig. 2(b) illustrates that the In nanoparticles are sphere and poly-sized with a wide range of particle sizes from 10 nm to 200 nm. The big difference of the particle size and distribution between the Cu and In nanoparticles can be explained from the reaction dynamics, as following. Basically, the synthesis reaction of Cu and In nanoparticles follows a simple oxide/reduction couple rule, in which Cu^{2+} or In^{3+} are reduced by the strong reductive agent $NaBH_4$. The potential gap between the couple controls the reaction potential. Comparing with the standard reduction potential ($E^{O}_{In^{3+}/In} = -0.338$ eV *vs* SHE (standard hydrogen electrode), $E^{O}_{Cu^{2+}/Cu} = 0.345$ eV *vs* SHE, $E^{O}_{B(OH)_3/BH_4^-} = -0.481$ eV *vs* SHE), it is clear that Cu^{2+} has a higher reaction potential to be reduced by $NaBH_4$ than In^{3+}. Thus, at the very beginning of the reaction, it is much quicker to form Cu nuclei, leading to a single nucleation event [16]. However, the much closer potential gap between In^{3+}/In and $B(OH)_3/BH_4^-$ can make a slower nucleation, leading to a multi-nucleation. In the growth period, the nuclei will grow bigger at the base of their initial sizes and distributions. Therefore, Cu nanoparticles from nuclei with similar sizes will follow a same growth period and display an approximate particle sizes. Whereas, In nanoparticles from nuclei with varied sizes have a much wider range of size distribution. Moreover, the higher diffusion rates of In in the solvent makes them easier to ripen, also leading to a much wider range of size distribution. Thus, the above-mentioned reaction mechanisms lead to the morphological difference between the Cu and In nanoparticles.

The XRD pattern shown in Fig. 1(c) elucidates that the Cu–In nanoparticles contain the two main phases of In (tetragonal, JCPDS-65-9682) and $Cu_{11}In_9$ (monoclinic, JCPDS-65-4963), which is consistent with the previous report that stable component phases of Cu–In alloy above 150 °C are mainly In and $Cu_{11}In_9$ [17]. In fact, we obtain the two component phases at a relative lower temperature of 140 °C. The obtained Cu–In nanoparticles are bigger in sizes due to the inter-diffusion of Cu and In nanoparticles [18], as indicated from the SEM image of a Cu–In metal film in Fig 4(a). It is considered that the polyol reaction might actualize some reactions which are difficult to happen in solid reactions [18]. However, we found that if the reaction temperature was over 150 °C the Cu–In nanoparticles would heavily agglomerate.

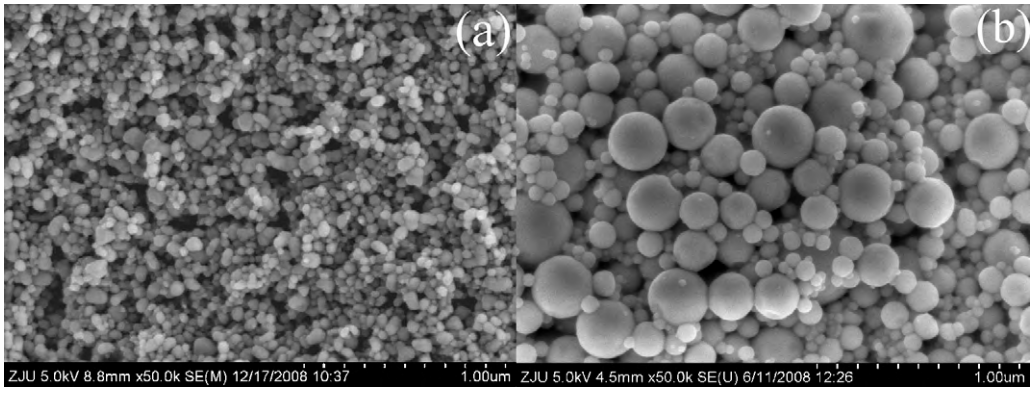

Fig. 2. SEM images of (a) Cu nanoparticles and (b) In nanoparticles by polyol method.

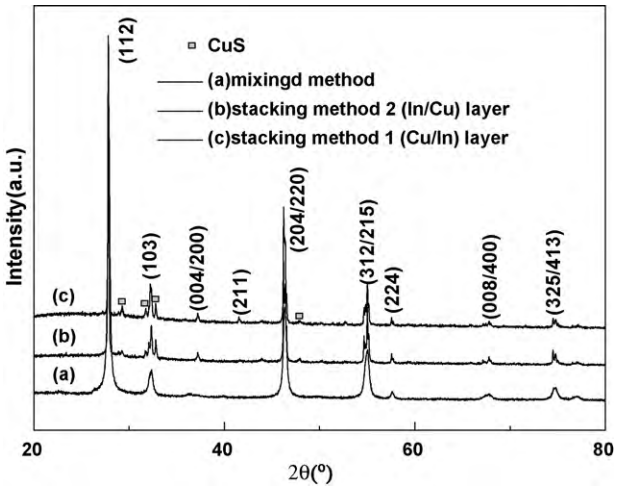

Fig. 3. XRD diffraction patterns of CIS films by (a) mixing method and (b) stacking method 2 (In/Cu layers) and (c) stacking method 1 (Cu/In layers).

After the synthesis of Cu, In and Cu–In nanoparticles, the corresponded inks are fabricated by dispersing the particles in solvents, which is mentioned in the section of experiment. And then, CIS films are formed by stacking and mixing methods and by sulfurization in sequence. The XRD patterns of the CIS films fabricated by three methods are shown in Fig. 3. It can be found that the main diffraction peaks of all the samples conform to the tetragonal phase of CIS (JCPDS-65-1572). Only single phase is observed in the film prepared by the mixing method, whereas some impurity phases of CuS can be found in the CIS films prepared by the two stacking methods. In the mixing method, the $Cu_{11}In_9$ phase in the Cu–In nanoparticles could be decomposed to $Cu_{16}In_9$ and liquid In at high temperatures, which may be beneficial for the sulfurization [19]. Thus, no distinct impurity phases are observed in the CIS film fabricated by the mixing method. In the mixing methods, although the inter-diffusion of Cu and In to form $Cu_{11}In_9$ phase dominates, some Cu and In nanoparticles in stacking layers may also be sulfurized ahead. In element may be evaporated in the form of indium sulfide (e.g. In_2S) at high temperature, leaving behind the impurity phase of CuS in the sulfurized samples [19,20], which plays an active role in the growth of CIS thin films [21]. Therefore, the impurity phase of CuS could be observed in the X-ray patterns of the films fabricated by the stacking methods. Moreover, it can be seen from Fig. 3 that no oxide phases can be detected in all the CIS films, indicating that during the nanoparticle synthesis, the PVP could slow down the oxidation rate of the synthesized Cu, In and Cu–In nanoparticles, as reported in Ref. [16,22].

The SEM image of the Cu–In metal film prepared by the mixing method before sulfurization is shown in Fig. 4(a). It can be seen that the Cu–In metal film is loose. After sulfurization, the CIS film is formed from the metal film, which is a compact film with large grain sizes, as shown in Fig. 4(b). Moreover, the cross-section SEM image of the films in Fig. 5(a) can also verify this. Compact films with thickness of over 3 μm can be obtained. The morphologies of the films prepared by the stacking methods are similar to that by the mixing method, which are not introduced. In the past decades, there have been many reports concentrating on the sulfurization of sputtering In/Cu stacking layer by either ex- or real-time techniques [19,20,23]. It has been well accepted that such sulfurization proceeds at the expense of $Cu_{11}In_9$ and is actually a surface reaction. The Cu and In atoms from $Cu_{11}In_9$ have to diffuse through the pre-formed CIS to react with S vapor. This can be verified from the cross-section SEM image of our atypical "extra-thick" Cu–In

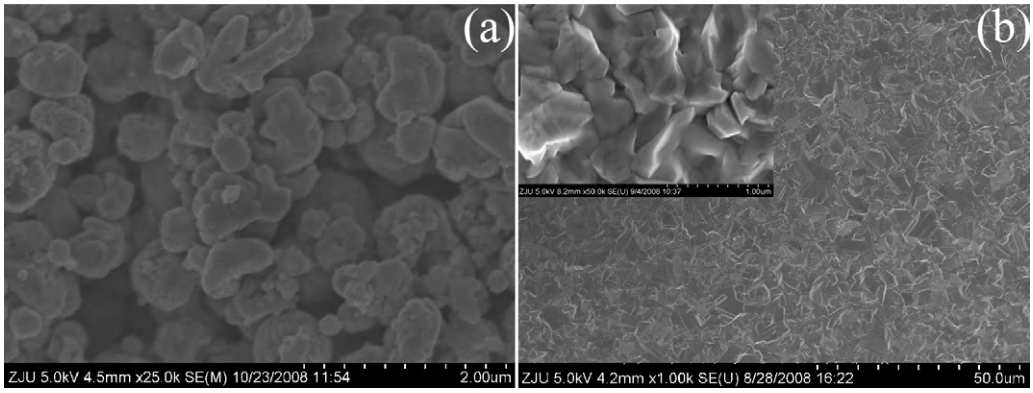

Fig. 4. SEM images of Cu–In metal films (a) before and (b) after sulfurization.

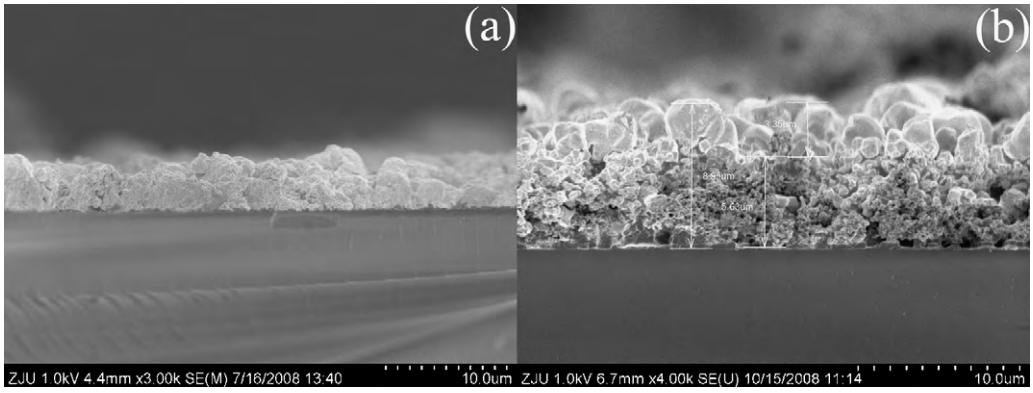

Fig. 5. Typical (a) and atypical (b) SEM cross-section images of the CIS films fabricated by the mixing method.

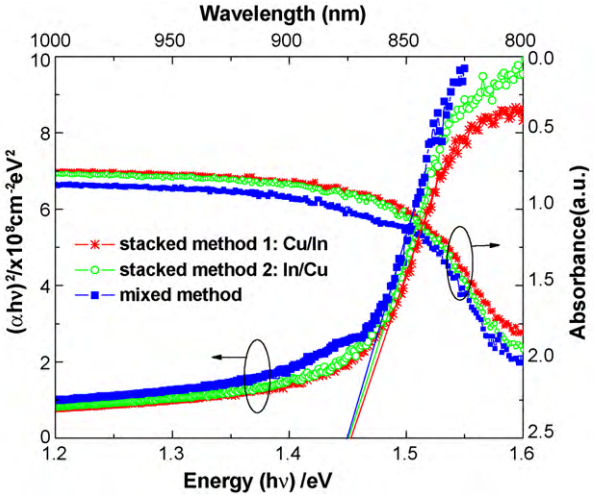

Fig. 6. Plot of absorbance against wavelength and $(\alpha h\nu)^2$ against photoenergy $(h\nu)$ of CIS films from different preparation methods of metal films.

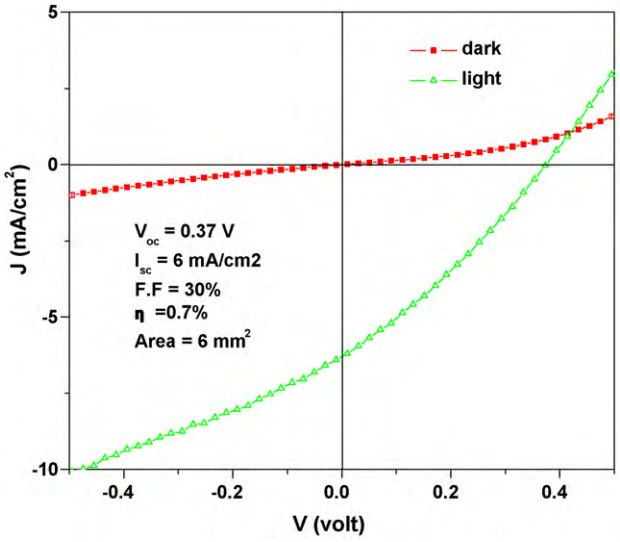

Fig. 7. Plot of current density *vs* voltage of the CIS solar cell.

nanoparticle films after sulfurization (Fig. 5(b)). In our experiments, the sulfurized films have two distinct layers. The top layer of about 3 μm thick is compact with large grain sizes, whereas the lower layer is loose with relatively small grains. In the extra-thick films, Cu and In atoms must march through a longer diffusion distances to be sulfurized on the surface, which is much more difficult. Therefore, sulfur must diffuse downward to the bottom to sulfur these atoms. The much lower sulfur pressure and shackled reaction place can result in the much smaller CIS grains. From this point of view, appropriate control of metal film thickness and sulfur pressure are very important to prepare qualified CIS films for solar cells.

The optical transmittances (T) of the obtained CIS films are measured by using a UV–vis spectrophotometer. The absorption coefficient (α) can be calculated from the relationship of transmittance (T) following the formula below [24]:

$$\alpha = \frac{\ln(1/T)}{d} \quad (1)$$

For simplicity, the direct characterization data of transmittance are demonstrated in the term of absorbance ($\ln(1/T)$). The absorbance spectrums of the CIS films fabricated by different methods are shown in Fig. 6. Moreover, the fundamental absorption, which manifests itself by a rapid rise in absorption, can be used to determine the energy gap (E_g) of a semiconductor. It is well known that $\alpha h\nu$ is proportional to $(h\nu - E_g)^m$, where $h\nu$ is the photon energy. Values of m for allowed direct and indirect, and forbidden direct and indirect optical transitions are 1/2, 2, 3/2 and 3, respectively. Thus, the band gaps are obtained by extrapolating the linear portion of the plots of $(\alpha h\nu)^{1/m}$ *versus* $h\nu$ to $\alpha^{1/m} = 0$. For an allowed direct transition ($m = 1/2$), α can be expressed as follows [25]:

$$\alpha = \left(\frac{A_1}{h\nu}\right)(h\nu - E_g)^{1/2} \quad (2)$$

where A_1 is a constant and E_g is the energy gap. The plot of $(\alpha h\nu)^2$ *versus* $h\nu$ is also drawn (Fig. 6) for the allowed direct band gap. The band gap E_G of 1.45 eV is determined from the extrapolated intercept with the Energy ($h\nu$) axis. It can be seen that E_G is nearly the same for all the films fabricated by different methods, which agrees with that of the CIS films synthesized with a similar method [26].

A typical CIS solar cell by the mixing method is fabricated with the conventional structure. The image in Fig. 7 shows the current–voltage characteristic of the solar cell, indicating that it exhibits a performance parameters of $V_{oc} = 0.37$ V, $I_{sc} = 6$ mA/cm^2, fill factor (F.F.) = 30% and efficiency (η) = 0.7%. We attribute the relative poor performance to the micro-cracks or pores due to the stresses in the sulfurization process. These cracks on one hand are beneficial for the sulfurization, but on the other hand may result in more leakage current paths and high contact resistance which are detrimental for the cell performances. In addition, the long sulfurization time we employed may also result in thick MoS_2 layer which can increase the series resistance of our devices. Therefore, careful control of the sulfurization is very important to improve the performances.

4. Conclusions

A simple chemical method to prepare Cu/In or Cu–In nanoparticles inks is developed. These metallic inks are applied to prepare CIS films. Both stacking and mixing methods are employed to prepare the metal films, corresponding to the two main states of art methods in industry. It is proven that all the methods based on our metal inks are feasible to prepare CIS films. Moreover, the $Cu_{11}In_9$ phase in the mixing method is beneficial for the sulfurization, exhibiting little impurity phases. CIS films by different methods similarly exhibit high absorption coefficient and appropriate E_G of 1.45 eV. CIS thin film solar cell by the mixing method is fabricated and obtained an efficiency of 0.7%.

Acknowledgements

The authors would like to appreciate the financial supports from 973 Project (No. 2007CB613403). We thank Jieru Wang and Guoliang Xu for their kind help for characterization and Jipeng Cheng for his deep discussion in experiments.

References

[1] N. Guezimir, T. Ben Nasrallah, K. Boubaker, M. Amlouk, S. Belgacem, J. Alloys Compd. 481 (2009) 543–548.
[2] C. Calderon, P. Bartolo-Perez, J. Clavijo, J.S. Oyola, G. Gordillo, Sol. Energy Mater. Sol. Cells 94 (2010) 17–21.
[3] A. Bollero, J.F. Trigo, J. Herrero, M.T. Gutierrez, Thin Solid Films 517 (2009) 2167–2170.
[4] F.M. Cui, L. Wang, Z.Q. Xi, Y. Sun, D.R. Yang, J. Mater. Sci.-Mater. Electron. 20 (2009) 609–613.
[5] N.K. Allouche, N. Jebbari, C. Guasch, N.K. Turki, J. Alloys Compd. 501 (2010) 85–88.
[6] S.J. Peng, F.Y. Cheng, J. Liang, Z.L. Tao, J. Chen, J. Alloys Compd. 481 (2009) 786–791.
[7] Z.D. Wang, X.L. Mo, J. Li, D.L. Sun, G.R. Chen, J. Alloys Compd. 487 (2009) L1–L4.

[8] L. Li, N. Coates, D. Moses, J. Am. Chem. Soc. 132 (2010) 22–23.
[9] H.W. Hillhouse, M.C. Beard, Curr. Opin. Colloid Interface Sci. 14 (2009) 245–259.
[10] S.Y. Lee, K.H. Kim, B.O. Park, Thin Solid Films 516 (2008) 4709–4712.
[11] T. Wada, H. Kinoshita, Thin Solid Films 480–481 (2005) 92–94.
[12] M. Kaelin, D. Rudmann, A.N. Tiwari, Sol. Energy 77 (2004) 749–756.
[13] B.M. Basol, Thin Solid Films 361–362 (2000) 514–519.
[14] G. Norsworthy, C.R. Leidholm, A. Halani, V.K. Kapur, R. Roe, B.M. Basol, R. Matson, Sol. Energy Mater. Sol. Cells 60 (2000) 127–134.
[15] Y.G. Sun, Y.N. Xia, Adv. Mater. 14 (2002) 833–837.
[16] B.K. Park, S. Jeong, D. Kim, J. Moon, S. Lim, J.S. Kim, J. Colloid Interface Sci. 311 (2007) 417–424.
[17] M. Gossla, H. Metzner, H.E. Mahnke, J. Appl. Phys. 86 (1999) 3624–3632.
[18] N.H. Chou, R.E. Schaak, J. Am. Chem. Soc. 129 (2007) 7339–7345.
[19] A. Joswig, M. Gossla, H. Metzner, U. Reislohner, T. Hahn, W. Witthuhn, Thin Solid Films 515 (2007) 5921–5924.
[20] M. Gossla, H.E. Mahnke, H. Metzner, Thin Solid Films 361–362 (2000) 56–60.
[21] J. Klaer, J. Bruns, R. Henninger, K. Seimer, R. Klenk, K. Ellmer, D. Braunig, Semicond. Sci. Technol. 13 (1998) 1456–1458.
[22] S. Jeong, K. Woo, D. Kim, S. Lim, J.S. Kim, H. Shin, Y.N. Xia, J. Moo, Adv. Funct. Mater. 18 (2008) 679–686.
[23] E. Rudigier, J. Djordjevic, C. von Klopmann, B. Barcones, A. Perez-Rodriguez, R. Scheer, J. Phys. Chem. Solids 66 (2005) 1954–1960.
[24] H.X. Tang, M. Yan, H. Zhang, X.Y. Ma, L. Wang, D.R. Yang, Chem. Res. Chinese U 21 (2005) 236–239.
[25] N. Kavcar, Sol. Energy Mater. Sol. Cells 52 (1998) 183–195.
[26] C.P. Liu, B.H. Tseng, Thin Solid Films 480–481 (2005) 50–54.